JOURNAL OF APPLIED PHYSICS **120**, 183902 (2016)

Exchange stiffness in ultrathin perpendicularly magnetized CoFeB layers determined using the spectroscopy of electrically excited spin waves

T. Devolder,[1,a)] J.-V. Kim,[1] L. Nistor,[2] R. Sousa,[2] B. Rodmacq,[2] and B. Diény[2]
[1]*Centre for Nanoscience and Nanotechnology, CNRS, University of Paris-Sud, Université Paris-Saclay, 91405 Orsay, France*
[2]*SPINTEC, UMR CEA/CNRS/UJF-Grenoble 1, Grenoble-INP, INAC, Grenoble F-38054, France*

(Received 19 September 2016; accepted 3 November 2016; published online 14 November 2016)

We measure the frequencies of spin waves in nm-thick perpendicularly magnetized FeCoB systems, and model the frequencies to deduce the exchange stiffness of this material in the ultrathin limit. For this, we embody the layers in magnetic tunnel junctions patterned into circular nanopillars of diameters ranging from 100 to 300 nm, and we use magneto-resistance to determine which rf-current frequencies are efficient in populating the spin wave modes. Micromagnetic calculations indicate that the ultrathin nature of the layer and the large wave vectors used ensure that the spin wave frequencies are predominantly determined by the exchange stiffness, such that the number of modes in a given frequency window can be used to estimate the exchange stiffness. For 1 nm layers, the experimental data are consistent with an exchange stiffness $A = 20 \pm 2$ pJ/m, which is slightly lower than its bulk counterpart. The thickness dependence of the exchange stiffness has strong implications for the numerous situations that involve ultrathin films hosting strong magnetization gradients, and the micromagnetic description thereof. *Published by AIP Publishing.*
[http://dx.doi.org/10.1063/1.4967826]

I. INTRODUCTION

The exchange interaction is fundamental to magnetism as it underpins the existence of ordered spin states. It determines the energy scale of excitations such as spin waves and the length scales in topological spin structures such as domain walls and vortices. Its strength establishes the extent to which ordered magnetic states are robust against thermal fluctuations, by governing quantities such as the Curie temperature at which the ferromagnetic-paramagnetic phase transition takes place. Quantifying the exchange interaction is therefore important for both fundamental studies and technological applications in which magnetic materials are used. For instance, the exchange stiffness is also expected to be critical to the thermal stability[1] of disks with perpendicular anisotropy layers, and thus, the exchange stiffness is of great importance in the development of spin-transfer-torque magnetic random access memories (STT-MRAM).

There exists a variety of experimental methods to determine the exchange stiffness, A. Many of them involve characterizing the spin wave dispersion. When the magnetic material extends till the outer surface of the sample, powerful surface techniques can be used to get the spin wave dispersion, such as spin polarized electron energy loss spectroscopy[2] and inelastic scanning tunnelling spectroscopy.[3] However in most systems of interest, the magnetic material is caped under functional layers and the aforementioned techniques are inoperative. For thin films with thicknesses greater than 10 nm, spin waves can be measured by neutron scattering,[4] inelastic X-ray scattering,[5] Brillouin light scattering,[6] and broadband ferromagnetic resonance using inductive methods.[7] Other methods include the direct use of Bloch's law.[8] For these thick systems, it is generally found that A is similar in magnitude to its bulk counterpart. However, since the exchange interaction involves the orbital overlap of the constituent magnetic atoms, the exchange stiffness A should be affected by the reduction in coordination number. This is a well established phenomenon in alloys[9,10] but should also be important in ultrathin films in which a larger proportion of the material is exposed to surfaces and interfaces. This has indeed been found for iron: an exchange stiffness of $A = 2 \pm 0.4$ pJ/m has been determined for an epitaxial monolayer of Fe sandwiched between Ir and Pd,[11] while a value of $A = 11.9 \pm 4$ pJ/m has been found for monolayer superlattices of Fe/Pt,[9,12] which are much lower than the iron bulk value of $A = 20$ pJ/m.[13]

For ultrathin films, scattering methods become less useful because they are not sufficiently sensitive to detect spin waves. Furthermore, techniques based on the Bloch law require extreme care as the thermal dependence of the magnetization is very sensitive to the range of the interactions and to the dimensionality of the system.[8,14–16] As such, many attempts to date have relied on spin textures with large magnetization gradients which require some assumptions on the form of the micromagnetic states involved and some insensitivity to structural disorder.[11,12,17] On the other hand, in magnetoresistive multilayers such as spin valve or magnetic tunnel junction (MTJ) nanopillars, it is possible to obtain signatures of the magnetization dynamics on lengths scales determined by the pillar geometry. For instance, estimates of A have been obtained in spin-transfer torque magnetic random access memories (STT-MRAM) by measuring the thermal stability and magnetization reversal involving spatially nonuniform processes,[18] and by characterizing the

[a)]thibaut.devolder@u-psud.fr

thermal noise of confined spin wave eigenmodes.[19] For these in-plane magnetized systems, it has been shown that there is a reduction of A with thickness from 20 pJ/m (bulk Fe) and 30 pJ/m (bulk Co) to 23 pJ/m for[19] 2 nm of $Fe_{40}Co_{40}B_{20}$ and 19 pJ/m for[18] 1.6 nm of $Fe_{56}Co_{19}B_{25}$.

However, an open question remains on how the exchange interaction evolves in ultrathin films with perpendicular magnetic anisotropy (PMA), such as nm-thick (Co,Fe) alloys in contact with heavy-metal underlayers and metal oxides, which underpin many studies on spin-orbit torques and interface-driven chiral interactions at present. In this article, we describe the exchange stiffness and its thickness dependence in a very popular PMA system: ultrathin CoFeB sandwiched between Ta and MgO. We deduce the exchange stiffness from the spectroscopy of electrically pumped spin waves in circular MTJ nanopillars. For 1 nm thick layers, the spin wave frequencies are consistent with an exchange stiffness of $A = 20 \pm 2$ pJ/m, which is found to be slightly lower than the bulk value of 27.5 pJ/m. The exchange stiffness is not found to decrease as dramatically as the magnetization with decreasing film thicknesses towards atomic dimensions.

II. SAMPLES

Our samples are magnetic tunnel junctions (MTJs) with perpendicular magnetic anisotropy (PMA). The stack composition is: buffer/Ta (5)/$Co_{60}Fe_{20}B_{20}$ ($t = 1$) (free layer)/MgO/$Co_{60}Fe_{20}B_{20}$ (1.6)/[Tb (0.4)/Co (0.5)]$_{\times 20}$/Ta (3)/Cu (3)/Ru (7), where the numbers in parentheses represent thicknesses in nm. The Tb/Co reference multilayer is a ferrimagnetic alloy, whose moment is nearly compensated (magnetization is 75 kA/m) to minimize the stray field acting on the free layer. The Tb/Co reference multilayer has a coercivity of 0.6 T, and an effective anisotropy above 1 T. This large anisotropy ensures that the spin waves in the reference layer have frequencies above 30 GHz, which can be neglected in the ensuing analysis since the free layer modes of interest lie in the range of 0–20 GHz (Fig. 2).

The free layer is crystallized[21] during an annealing step that is accompanied by a partial diffusion of the B atoms towards the Ta layer, leaving a free layer whose composition lies between $Co_{75}Fe_{25}$ and $Co_{60}Fe_{20}B_{20}$. The B interstitial atoms are known not to affect substantially the exchange stiffness which is $A = 27.5$ pJ/m in the bulk for our CoFeB composition.[7] The layers were not found to be ferromagnetic at room temperature for thickness below 0.5 nm, and exhibited PMA for thickness up to 1.2 nm. We do not make any assumptions on the presence of any magnetically "dead" layers, so the free layer magnetization is defined as the areal moment divided by the nominal thickness. Note that for consistency, if we were to assume a dead layer and the related weakly magnetic Fe and Co atoms, we would necessarily need to also assume a layer-resolved exchange stiffness, which is impossible in a micromagnetic approach, hence beyond the scope of this paper. The magnetizations were measured by vibrating sample magnetometry and were found to increase linearly from $M_S = 0.6$ MA/m for 1 nm thick layers to a plateau with a bulk value (1.4 MA/m) for thicknesses above 1.5 nm. The tunnel magnetoresistance is typically $\eta_{tmr} = 50\%$. The stack resistance-area product is $RA = 14\ \Omega\,\mu m^2$.

The PMA MTJs were patterned into circular pillars with nominal diameters $2a$ of 100, 200, and 300 nm. For the set of devices studied, the mean device resistances were found to be correlated with their nominal size, but the slight offset in the values observed suggests a radius reduction of 2–15 nm during the process. From past studies on in-plane magnetized samples and their shape anisotropy, we have evidence that our fabrication process yields junctions that are essentially circular. Hence, in the remainder of this study, we will assume an exact junction radius defined by $a = \sqrt{RA/(\pi R_p)}$. This leads to typical resistances of 200 Ω ($a = 150$ nm) to 1800 Ω ($a = 50$ nm) in the parallel (P) state.

III. EXPERIMENTAL CONSIDERATIONS

A. Experimental set-up

The pillars are characterized in an spin–transfer–torque ferromagnetic resonance (STT-FMR)-like[22] set-up (Fig. 1). The objective is to reveal the frequency versus field dispersion laws of the spin waves of the free layer. The device is biased using a dc source supplying $V_{dc} = \pm 1$ mV and fed with an RF voltage supplying $V_{rf} \approx 350\,mV_{pp}$ at a variable frequency $3 \leq \omega_{rf}/(2\pi) \leq 20$ GHz. The RF voltage is pulse-modulated at an ac frequency $\omega_{ac}/(2\pi) = 50$ kHz (Fig. 1) such that the current passing through the MTJ has frequency components at the two sidebands $\omega_{rf} \pm \omega_{ac}$.

The spin waves are populated by the RF torques, i.e., the STT, along with the current-induced fields that are generated by the microwave circuitry used to probe the device. A proper demodulation of the *ac* voltage across the device yields a signal containing magnetic susceptibility information. For each applied field, the signal exhibits marked extrema at well defined frequencies (Fig. 1) that we shall demonstrate to correspond to spin wave modes in the free layer.

B. Origin of the demodulated signals

The demodulated signal can contain two *ac* components V_1 and V_2 (Fig. 1) of different physical origins. The first expected *ac* component is the standard STT-FMR signal: the *rf* current is at the frequencies $\omega_{rf} \pm \omega_{ac}$ and it rectifies to *ac* any oscillation of the resistance δr_{rf} occurring at the frequency ω_{rf}. However, because of the cylindrical symmetry of our configuration—PMA and applied field collinear to the easy axis—the magnetization precession associated with a spin wave is supposed not to make the device resistance oscillate at the precession frequency: we expect $\delta r(\omega_{rf}) = 0$. The STT-FMR signal V_1 should thus vanish, in line with the conclusions in Ref. 23.

The second *ac* signal (V_2) is a much larger signal related to the decrease of the time-averaged magnetization due to the spin wave populations. Indeed, when the RF torques are applied, the spatially and temporally averaged magnetization $|\langle M_z \rangle|$ of the free layer is less than its value M_S in the saturated states. The correlated change of resistance δr_{ac} is revealed by the small dc current I_{dc} passing through the sample, i.e.,

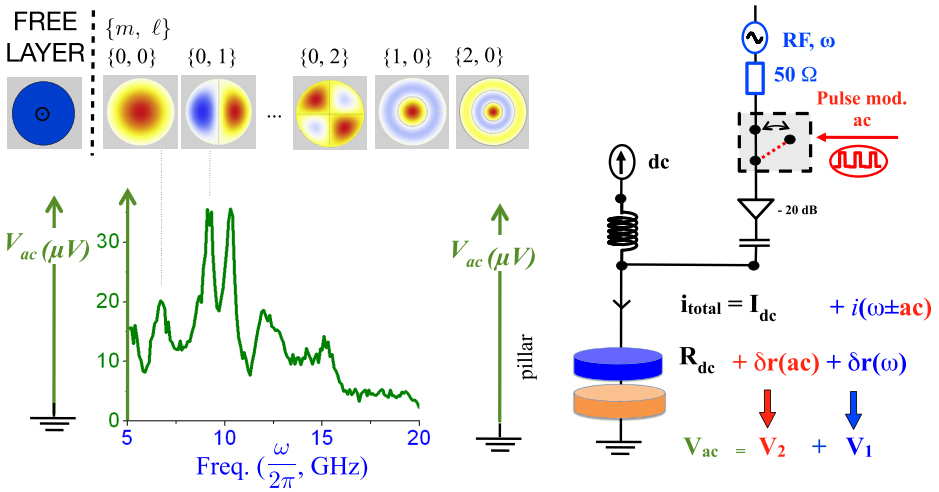

FIG. 1. Illustration of the method and sketch of the set-up. Right: the pillar is biased with a dc voltage and an RF voltage undergoing an on/off modulation at an ac frequency. The pillar resistance differs when the RF is on or off. Thanks to the dc current, this creates an ac voltage drop V_2 which is peaked (bottom left) whenever the applied rf frequency hits a spin wave frequency. Since our applied field and magnetization are collinear, the spin waves are not accompanied with a synchronous change of the sample resistance ($\delta r = 0$) and the conventional STT-FMR signal V_1 cancels. Top left: examples of the x component of the dynamic magnetization of some of the eigenmodes of a uniformly magnetized free layer disk (blue) according to the analytical frameworks.[20] The superimposed dashed lines are the nodal lines.

$$V_2 \propto I_{dc} \times (\langle M_z \rangle - M_S)\,. \tag{1}$$

Note that the rectified voltage V_2 due to the rf-torque-induced change of the spin-wave population changes sign with the sign of the bias current I_{dc} and with free layer switching. This is in line with our finding (see the left-right contrast is Fig. 2 when the magnetization of the free layer switches).

C. Amplitude of the signal associated with the spin wave population

The order of magnitude of V_2 can be assessed from simple arguments. The rf Oersted field at the device edge (i.e., at $r = a$) is

$$H_{\mathrm{Oe},\perp} \approx V_{rf}.a/RA, \tag{2}$$

which yields typically a few kA/m. The local susceptibility at resonance has an order of magnitude that is comparable to that of the macrospin approximation[24]

$$\chi = \frac{M_S}{2\alpha\left(\dfrac{2K_s}{\mu_0 M_S t} - M_S\right)}, \tag{3}$$

which is typically 20–50. K_s is the interface anisotropy and α is the damping factor. Overall, this yields a signal transduction of the order of

$$\frac{V_2}{V_{dc}} \approx \eta_{tmr}\chi\frac{H_{\mathrm{Oe},\perp}}{M_S} \tag{4}$$

that provides $V_2 \approx 20$ to $50\,\mu V_{ac}$ for the most uniform eigenmodes in the largest junctions. This signal decreases

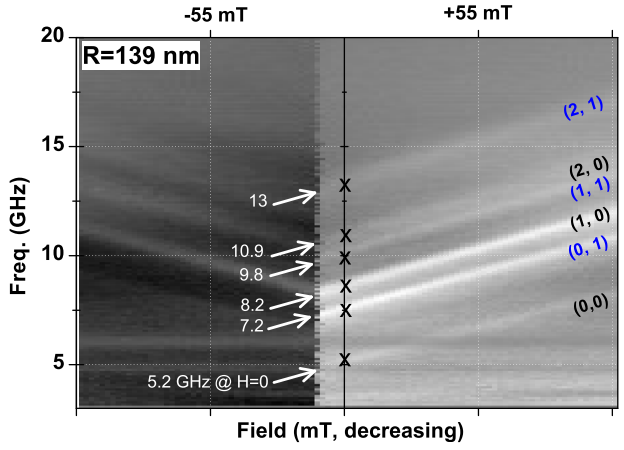

FIG. 2. Rectified voltage versus field and frequency for a nanopillar of radius 139 nm and a free layer of thickness 10 Å biased with $V_{dc} = -1$ mV. The field is decreased from 110 mT (AP state) to −110 mT. The pixelized line of color change at −13 mT is the switching to the P state. The superimposed labels recall the proposed mode indexation. The quoted frequencies correspond to the zero field point.

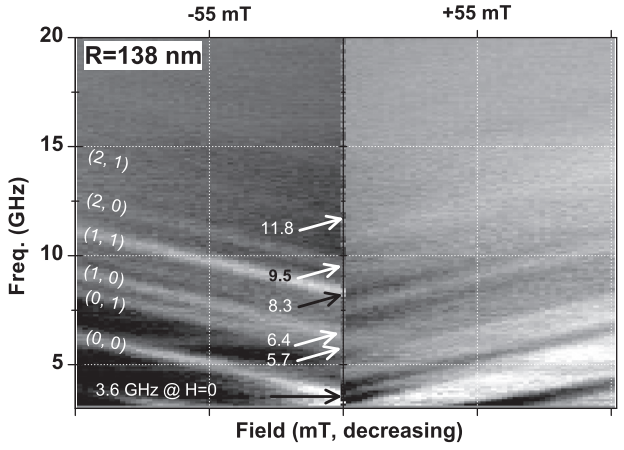

FIG. 3. Rectified voltage versus field and frequency for a nanopillar of radius 138 nm and a free layer of thickness 10.5 Å biased with $V_{dc} = +1$ mV. The field is decreased from 110 mT (AP state) to −110 mT. The pixelized line of color change at −1 mT is the switching to the P state. The superimposed labels recall the proposed mode indexation. The quoted frequencies correspond to the zero field point.

when devices are shrunk because the rf Oersted field diminishes with the device diameter (see Eq. (2)).

IV. EXPERIMENTAL RESULTS

To check that the signal extrema are not artefacts due to impedance mismatches and the related standing waves in the circuitry, we vary the applied magnetic field. This is, for instance, done in Figs. 2 and 3 for large MTJs with 10 Å and 10.5 Å thick free layers, and in Figs. 4 and 5 for devices of smaller diameters and free layer of thickness 10 Å. Four main points are worth noticing in these figures.

(1) The spin wave dispersion relations appear as V-shaped branches, with a slope inversion when the magnetization of the FeCoB free layer switches. This slope inversion confirms that the observed spin waves are hosted by the free layer. The peak frequency linewidths $\Delta\omega$ are consistent with a free layer effective damping of $\Delta\omega/(2\omega) = 0.03-0.04$, depending on the device.
(2) For a given device diameter, the spin waves gradually move to lower frequencies as the free layer thickness is increased, and the effective anisotropy is consequently lowered (Fig. 3). The spin wave branches are linear for samples showing PMA. The spin wave branches bend in a complex manner (not shown) for thicker samples when the magnetization partially tilts towards the in-plane direction.
(3) When reducing the device diameters (Figs. 4 and 5), this increases the lateral confinement of the spin waves which consequently increases the exchange contribution to their frequencies. As a result, the frequency spacing between the spin wave branches increases.
(4) In addition, the switching of the free layer results also in a drastic change of the signal amplitude that can be noticed as a left-side versus right-side contrast in Fig. 2. While the modes are clearly identified for one field polarity, their identification is systematically much more difficult for the other field polarity. This drastic dependence of the demodulated signal on the free layer orientation is informative on the nature of the mechanism that populates the observed spin waves. Let us thus discuss the origin of our signals using the available analytical models.

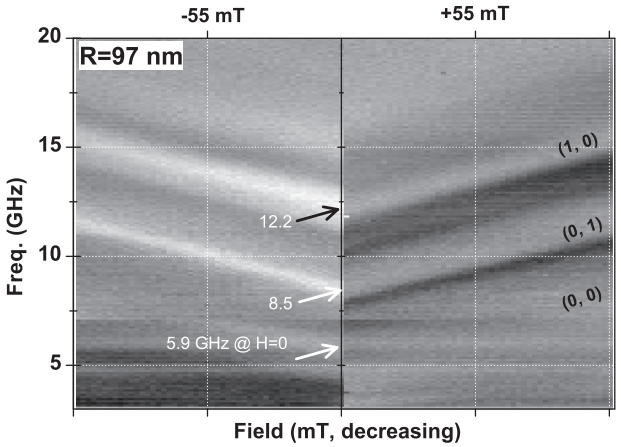

FIG. 4. Rectified voltage versus field and frequency for a nanopillar of radius 97 nm and a free layer of thickness 10 Å biased with $V_{dc} = +1$ mV. The superimposed labels recall the proposed mode indexation. The quoted frequencies correspond to the zero field point.

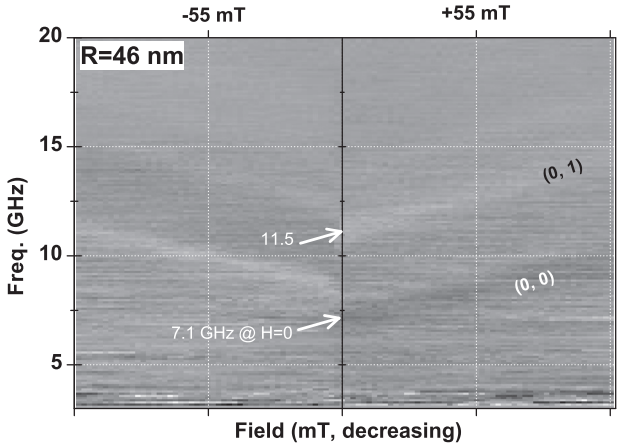

FIG. 5. Rectified voltage versus field and frequency for a nanopillar of radius 46 nm and a free layer of thickness 10 Å biased with $V_{dc} = +1$ mV. The superimposed labels recall the proposed mode indexation. The quoted frequencies correspond to the zero field point.

V. EXPECTATIONS FROM THE APPROXIMATE ANALYTICAL MODELS

Let us now describe our expectations concerning the nature of the observed spin waves. The eigenmodes of perpendicularly magnetized circular disks are well understood.[20,23,25] As sketched in Fig. 1, the modes can be referred to by their radial index $m \in \mathbb{N}$, where m is the number of nodes along the radial axis and $\ell \in \mathbb{Z}$ is the winding number which describes the number of magnetization turns along any path encompassing the disk center.

The modes $\{m, 0\}$ are the purely radial modes of symmetries $\{\bigcirc\ \circledcirc\ \circledcirc\ \circledcirc\}$ where the lines denote the nodes that separate regions of dynamical magnetizations with opposite signs. The azimuthal index $\{\ell = 1, 2, ...\}$ adds nodal lines $\{\ominus, \oplus, ...\}$ along the sample diameters (see some examples in Fig. 1).

In isolated perfectly circular disks with PMA, the $\{m, \ell\}$ and $\{m, -\ell\}$ modes are predicted to be fully degenerate in the absence of magneto-static interactions.[25] In perfectly circular disks, their degeneracy can be lifted by effects with a winding symmetry, like a static orthoradial Oersted field or a radially divergent stray field coming from the reference layers. In our case, these two fields have a marginal contribution to the $|\ell| = 1$ mode frequencies that we can neglect considering the much larger value of the mode linewidths. Similar arguments apply to maintain the pair degeneracy of the higher order modes with $|\ell| \geq 2$. In short, we do not expect to be able to separate the azimuthal modes $\{m, \ell\}$ and $\{m, -\ell\}$, and we will thus sort our modes with $\ell \geq 0$ only.

The different spatial profiles of the spin wave modes (Fig. 1) confer to them different susceptibilities to the rf torques present in our configuration. The rf current flowing through the electrodes generates a small quasi-uniform rf field h_x on the device. This field can excite the purely radial $\{m, 0\}$ modes, but the excitation efficiency decreases with m.

This parasitic pumping field h_x is rather uniform at the scale of the device such that it should only excite the purely radial modes. Conversely, the rf Oersted field has a $|\ell| = 1$ symmetry and thus excites predominantly the $\{m, 1\}$ modes. It has a strong radial gradient which provides a priori an excitation route for all values of m. Since the dynamic Oersted field provides the largest torque in our configuration,[23] we expect the strongest signal from the $\{m, 1\}$ modes. We have not identified any mechanism to excite the $\ell \geq 2$ modes in our experimental configuration.

The frequencies of the spin waves can be predicted semi-quantitatively using the models of Refs. 23 and 25. Writing the effective wavevectors $k_{m,\ell}$ such that $ak_{m,\ell}$ is the mth zero of the ℓth Bessel's function,[20] the spin wave frequencies can be expressed as

$$\omega_m^2/\gamma_0^2 = H_1 H_2, \tag{5}$$

with the two stiffness fields being

$$H_1 = H_z + \frac{2K_s}{\mu_0 M_S t} - N_{m,\ell} M_S + \frac{2Ak_{m,\ell}^2}{\mu_0 M_S}, \tag{6}$$

and

$$H_2 = H_1 + M_S\left(1 - \frac{1 - e^{k_{m,\ell}L}}{k_{m,\ell}L}\right). \tag{7}$$

While the last term in Eq. (7) is the same as in infinite films,[26] the factor $N_{m,\ell}$ is a mode dependent demagnetizing factor that accounts mainly for the reduction of the demagnetizing field in the out-of-plane direction as the disk radius is reduced. The demagnetizing terms for the purely radial modes $\{m, 0\}$ can be calculated analytically,[27] but micromagnetics is unavoidable for the azimuthal modes.

VI. SPIN WAVE FREQUENCIES AND PROFILES FROM MICROMAGNETICS

We have thus used micromagnetic simulations (mumax3,[28]) to take into account the magnetostatic interactions in an exact manner. To compute the eigenmode spectrum of, for instance, the largest disks (diameter 278 nm, representative of our set of experimental data), we first calculate an initial ground state for the free layer after discretization onto 256×256 finite difference points. This ground state is thermalized at 300 K to give nonuniform modes a finite susceptibility to the uniform rf fields. We then compute the 25 ns long transient response to a uniform in-plane field impulse formed by a cardinal sinus function with 50 GHz cutoff. The mode profiles are finally identified using a finite-element discretization (256 finite elements) that speeds up calculation in a manner to be described elsewhere. The procedure was repeated systematically for exchange stiffnesses from 10 to 30 pJ/m (Fig. 6).

Compared to the trial eigenmode profiles used in the analytical frameworks (Fig. 1 and Refs. 20, 23, and 25), the micromagnetics mode profiles (Fig. 6) are distorted and show a trend towards more localization near the sample edges. Linked with this localization, the influence of exchange interaction on

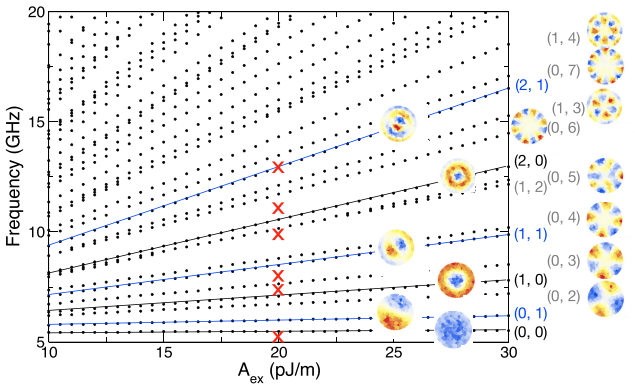

FIG. 6. Dependence of the micromagnetically calculated eigenmode frequencies (dots and lines as guide to the eye) versus exchange stiffness for circular disks of radius 138 nm, thickness 10 Å, anisotropy 0.28 MJ/m^3, and magnetization 0.6 MA/m, mimicking the sample on which Fig. 2 was recorded. The colored wheels illustrate the spatial profiles of each simulated mode. The red crosses are the experimentally detected frequencies.

the eigenmode frequencies (Eq. (6)) is altered and the spacing between the frequencies does not appear to increase proportionally to the exchange stiffness (notice for instance the weak dependence on the exchange stiffness of the spacing between the modes (0, 0) and (0, 1) in Fig. 6). As a result, the sole mode-to-mode frequency distances cannot be used as a measure of A/M_s, contrary to what the (approximate) Eq. (5) would imply. Micromagnetic effects seem to render this approach unquantitative. The deficiencies of Eqs. (6) and (7) do however not impede the mode indexation. Indeed, even in full micromagnetics (Fig. 6), the frequencies of the modes are still ordered as they would be in the analytical frameworks (Eq. (5)) according to their exchange terms $\frac{2Ak_{m,\ell}^2}{\mu_0 M_S}$. As such, the modes always appear in the same order. Keeping only the modes with $\ell \leq 1$, the order is predicted to be

$$\omega_{(0,0)} < \omega_{(0,1)} < \omega_{(1,0)} < \omega_{(1,1)} < \omega_{(2,0)} < \omega_{(2,1)}.$$

Looking back at the experimental results, the lowest frequency mode [labeled (0,0)] led statistically to a low rectified signal. The two next modes [labeled (0,1) and (1,0)] led generally to the largest response. The weak (0,0) mode is logically the response to the (weak) rf field h_x, and the intense (0,1) mode is the response to the (larger) rf Oersted field. The next mode, labeled (1,0) and of radial character, is more intense than anticipated, as if the pinning conditions at the device edge were much more relaxed compared to expectations.

We have conducted this analysis for several device sizes with 1 nm thick free layers. In the frequency window [5, 15 GHz], we usually found 6 modes for devices of radii in the range of 140 nm, 4 modes for radii 100 nm, and 2 modes for radii 50 nm. The experimental frequencies are spread from sample to sample, which indicates that the pinning conditions at the edges differ from device to device, probably as a result of the damages induced during the patterning process. As shown in Fig. 6, the observed frequencies do not generally match with the one predicted by micromagnetics; there is no value of A that would provide a perfect agreement between

micromagnetics and the experimental data. However, with the measured areal moments and the nominal thicknesses, the exchange stiffness leading to 6 observable (i.e., with $\ell \leq 1$) modes in our measurement window was found to be 20 ± 2 pJ/m for 10 Å thick free layer. Despite our sizable error bar of ± 2 pJ/m, we can conclude that the exchange stiffness in the ultrathin limit is lower than that of the bulk state (27.5 pJ/m). Noticeably, its decay with the free layer thickness seems much slower than the magnetization and does not follow the $A \propto M_S^2$ trend generally observed in bulk systems.[5]

VII. CONCLUSION

In summary, we have measured the frequencies of spin waves of large wavevectors in nm-thick perpendicularly magnetized CoFeB systems. The measurement method relies on magneto-resistance to enable the spectroscopy of rf-current populated spin waves in nanopillars of deep submicron size. The ultrathin nature of the films and the large wavevectors used ensure that the spin wave frequencies are primarily determined by the intralayer exchange stiffness. However, micromagnetic effects impede a direct and analytical calculation of the exchange stiffness from the mode frequency spacings. Using micromagnetics, a proper mode indexation allows to deduce that the exchange stiffness of the CoFeB free layer is around $A = 20 \pm 2$ pJ/m, which is 30% less than its bulk counterpart. The decrease in magnetization at low thickness is much more pronounced, such that the exchange length should be longer in the ultrathin films than in their bulk counterpart. This unexpected thickness evolution of the exchange stiffness has strong implications for the vast class of physical problems involving strong magnetization gradients in ultrathin films.

ACKNOWLEDGMENTS

We thank Felipe Garcia-Sanchez and Grégoire de Loubens for fruitful discussions. This work was supported by the French National Research Agency (ANR) under Contract Nos. ANR-11-BS10-0003 (NanoSWITI) and ANR-14-CE26-0012 (ULTRASKY).

[1]G. D. Chaves-O'Flynn, G. Wolf, J. Z. Sun, and A. D. Kent, Phys. Rev. Appl. **4**, 024010 (2015).
[2]R. Vollmer, M. Etzkorn, P. S. A. Kumar, H. Ibach, and J. Kirschner, Phys. Rev. Lett. **91**, 147201 (2003).
[3]A. Spinelli, B. Bryant, F. Delgado, J. Fernndez-Rossier, and A. F. Otte, Nat. Mater. **13**, 782 (2014).
[4]H. A. Alperin, O. Steinsvoll, G. Shirane, and R. Nathans, J. Appl. Phys. **37**, 1052 (1966).
[5]M. Mulazzi, A. Chainani, Y. Takata, Y. Tanaka, Y. Nishino, K. Tamasaku, T. Ishikawa, T. Takeuchi, Y. Ishida, Y. Senba, H. Ohashi, and S. Shin, Phys. Rev. B **77**, 224425 (2008).
[6]X. Liu, M. M. Steiner, R. Sooryakumar, G. A. Prinz, R. F. C. Farrow, and G. Harp, Phys. Rev. B **53**, 12166 (1996).
[7]C. Bilzer, T. Devolder, J.-V. Kim, G. Counil, C. Chappert, S. Cardoso, and P. P. Freitas, J. Appl. Phys. **100**, 053903 (2006).
[8]H. T. Nembach, J. M. Shaw, M. Weiler, E. Ju, and T. J. Silva, Nat. Phys. **11**, 825 (2015).
[9]C. Antoniak, J. Lindner, K. Fauth, J.-U. Thiele, J. Minr, S. Mankovsky, H. Ebert, H. Wende, and M. Farle, Phys. Rev. B **82**, 064403 (2010).
[10]C. Eyrich, A. Zamani, W. Huttema, M. Arora, D. Harrison, F. Rashidi, D. Broun, B. Heinrich, O. Mryasov, M. Ahlberg, O. Karis, P. E. Jnsson, M. From, X. Zhu, and E. Girt, Phys. Rev. B **90**, 235408 (2014).
[11]N. Romming, A. Kubetzka, C. Hanneken, K. von Bergmann, and R. Wiesendanger, Phys. Rev. Lett. **114**, 177203 (2015).
[12]S. Okamoto, N. Kikuchi, O. Kitakami, T. Miyazaki, Y. Shimada, and K. Fukamichi, Phys. Rev. B **66**, 024413 (2002).
[13]J. F. Cochran, in *Ultrathin Magnetic Structures II*, edited by B. Heinrich and J. A. C. Bland (Springer, 1994).
[14]N. D. Mermin and H. Wagner, Phys. Rev. Lett. **17**, 1133 (1966).
[15]U. Krey, J. Magn. Magn. Mater. **268**, 277 (2004).
[16]W. Kipferl, M. Dumm, P. Kotissek, F. Steinbauer, and G. Bayreuther, J. Appl. Phys. **95**, 7417 (2004).
[17]N. Sato, R. M. White, and S. X. Wang, Appl. Phys. Lett. **108**, 152405 (2016).
[18]H. Sato, M. Yamanouchi, K. Miura, S. Ikeda, R. Koizumi, F. Matsukura, and H. Ohno, IEEE Magn. Lett. **3**, 3000204 (2012).
[19]T. Devolder, L. Bianchini, K. Miura, K. Ito, J.-V. Kim, P. Crozat, V. Morin, A. Helmer, C. Chappert, S. Ikeda, and H. Ohno, Appl. Phys. Lett. **98**, 162502 (2011).
[20]O. Klein, G. de Loubens, V. V. Naletov, F. Boust, T. Guillet, H. Hurdequint, A. Leksikov, A. N. Slavin, V. S. Tiberkevich, and N. Vukadinovic, Phys. Rev. B **78**, 144410 (2008).
[21]Y. M. Lee, J. Hayakawa, S. Ikeda, F. Matsukura, and H. Ohno, Appl. Phys. Lett. **89**, 042506 (2006).
[22]A. A. Tulapurkar, Y. Suzuki, A. Fukushima, H. Kubota, H. Maehara, K. Tsunekawa, D. D. Djayaprawira, N. Watanabe, and S. Yuasa, Nature **438**, 339 (2005).
[23]V. V. Naletov, G. de Loubens, G. Albuquerque, S. Borlenghi, V. Cros, G. Faini, J. Grollier, H. Hurdequint, N. Locatelli, B. Pigeau, A. N. Slavin, V. S. Tiberkevich, C. Ulysse, T. Valet, and O. Klein, Phys. Rev. B **84**, 224423 (2011).
[24]T. Devolder, P.-H. Ducrot, J.-P. Adam, I. Barisic, N. Vernier, J.-V. Kim, B. Ockert, and D. Ravelosona, Appl. Phys. Lett. **102**, 022407 (2013).
[25]K. Munira and P. B. Visscher, J. Appl. Phys. **117**, 17B710 (2015).
[26]B. A. Kalinikos and A. N. Slavin, J. Phys. C: Solid State Phys. **19**, 7013 (1986).
[27]N. Ross, M. Kostylev, and R. L. Stamps, J. Appl. Phys. **116**, 113909 (2014).
[28]A. Vansteenkiste, J. Leliaert, M. Dvornik, M. Helsen, F. Garcia-Sanchez, and B. V. Waeyenberge, AIP Adv. **4**, 107133 (2014).